AIP | Review of Scientific Instruments

A flux extraction device to measure the magnetic moment of large samples; application to bulk superconductors

R. Egan, M. Philippe, L. Wera, J. F. Fagnard, B. Vanderheyden, A. Dennis, Y. Shi, D. A. Cardwell, and P. Vanderbemden

Citation: Review of Scientific Instruments **86**, 025107 (2015); doi: 10.1063/1.4907903
View online: http://dx.doi.org/10.1063/1.4907903
View Table of Contents: http://scitation.aip.org/content/aip/journal/rsi/86/2?ver=pdfcov
Published by the AIP Publishing

A flux extraction device to measure the magnetic moment of large samples; application to bulk superconductors

R. Egan,[1] M. Philippe,[1] L. Wera,[1] J. F. Fagnard,[1] B. Vanderheyden,[1] A. Dennis,[2] Y. Shi,[2] D. A. Cardwell,[2] and P. Vanderbemden[1]
[1]*SUPRATECS and Department of Electrical Engineering and Computer Science B28, Sart-Tilman, B-4000 Liège, Belgium*
[2]*Bulk Superconductivity Group, Engineering Department, Cambridge University, Cambridge CB2 1PZ, United Kingdom*

(Received 10 December 2014; accepted 28 January 2015; published online 13 February 2015)

We report the design and construction of a flux extraction device to measure the DC magnetic moment of large samples (i.e., several cm^3) at cryogenic temperature. The signal is constructed by integrating the electromotive force generated by two coils wound in series-opposition that move around the sample. We show that an octupole expansion of the magnetic vector potential can be used conveniently to treat near-field effects for this geometrical configuration. The resulting expansion is tested for the case of a large, permanently magnetized, type-II superconducting sample. The dimensions of the sensing coils are determined in such a way that the measurement is influenced by the dipole magnetic moment of the sample and not by moments of higher order, within user-determined upper bounds. The device, which is able to measure magnetic moments in excess of 1 A m^2 (1000 emu), is validated by (i) a direct calibration experiment using a small coil driven by a known current and (ii) by comparison with the results of numerical calculations obtained previously using a flux measurement technique. The sensitivity of the device is demonstrated by the measurement of flux-creep relaxation of the magnetization in a large bulk superconductor sample at liquid nitrogen temperature (77 K). [http://dx.doi.org/10.1063/1.4907903]

I. INTRODUCTION

Large, single grain bulk high-temperature superconductors (HTSs) fabricated by the so-called top seeded melt growth (TSMG) processing technique have the greatest field-trapping ability of any known material.[1,2] As a result, these materials are attracting increasing interest for many applications in which they can act effectively as strong quasi-permanent magnets, including rotating machines[3] and stable magnetic levitation devices.[4] Bulk superconducting magnets consist typically of cylinders of 10–50 mm in diameter and 10–20 mm in height.[5] Associated measurement and characterization methods by both destructive and non-destructive techniques have developed naturally as the ability to melt process these materials has evolved. Of these, the most popular methods have tended to focus on local measurements of the flux density by scanning a miniature Hall probe above the top surface of the sample, either after full magnetization of the sample by a field cooling technique[6–8] or by using a small permanent magnet moved simultaneously with the Hall probe (the so-called "magnetoscan" technique).[9] Such measurement techniques have provided valuable information about current distribution and characteristics in the vicinity of the surface of the sample, although they are significantly less sensitive to the inner, bulk critical current density.

Bespoke AC susceptometers can be used to investigate the volumetric properties of large superconducting samples,[10–12] although the penetration depth of the largest AC fields (0.1 T) at temperatures of interest (e.g., 77 K or lower) in high quality materials is typically small compared to the diameter of the sample.[10] One method of measuring the volume DC magnetic properties of these large, bulk superconductors involves winding a coil tightly around the sample and then measuring the flux in the coil directly.[13] Unfortunately, however, this method only provides information about the average magnetic flux density in the sample,[14] and the determination of the magnetic moment requires numerical modeling based on assumptions concerning isotropy, homogeneity, and constitution.[13] In order to avoid such limitations and complications, an appropriate magnetometer should be employed if the DC magnetic moment of the sample is to be determined independently of any other property of the sample.

It should be emphasized within this context that well established magnetometers, including vibrating sample/coil,[15,16] flux extraction,[17–19] and SQUID devices, measure typically the magnetic moment of samples that are much less than 1 cm^3 in volume,[20,21] which is up to two orders of magnitude smaller than the typical dimensions of state of the art melt processed HTS samples. Moreover, since the design and calibration of these measurement techniques rely fundamentally on a dipole hypothesis for the sample, they are generally accurate only for samples that are much smaller than the radius of the sensing coils or for uniformly magnetized samples of a specific, well defined geometry.[15–19,22–24]

Various approaches have been proposed over the past two decades to enable meaningful magnetization measurements to be performed on samples of size comparable with that of the sensing coils. The first of these is associated with vibrating

sample magnetometry (VSM) and consists of designing a coil arrangement to flatten and optimize its sensitivity function selectively at the location of the sample.[16,25,26] However, fundamental to this technique is the assumption of a homogeneous sample magnetization and an increased complexity of the coil arrangement, which impedes its practical application for large samples. Simpler alternatives have been also considered, including (i) the modification of a calibration constant by assuming a specific sample shape and a homogeneous magnetization[17,27,28] and (ii) the use of deconvolution techniques to determine the magnetization distribution of extended samples along their major geometrical axis.[29,30] Unfortunately, these methods are not applicable to the measurement of bulk superconducting magnets because (i) the assumption of a homogeneous magnetization state does not hold and (ii) they cannot be described as extended samples given that their radius can be comparable with their height.

In this paper, we propose a device designed to measure the magnetic moment of magnetized bulk samples of a few cm^3 in volume, including bulk HTS, melt processed disks. A flux extraction technique is preferred to vibrating techniques primarily for mechanical simplicity. The system is designed by making use of a multipole expansion, as proposed elsewhere.[31] The present approach, however, differs by making use of a tensor expansion rather than vector spherical harmonics and has the advantage of making a connection between the contributions associated with high order magnetic moments, on one hand, and the tensor contraction between sample-related and coil-related tensors, on the other. As a result, the technique reported here addresses directly the problem of sample misalignment, which would otherwise require complex calculations and also encompass previous specific results, but in a very general way. Although the present work focuses on cylindrical samples, the fundamental technique can be extended easily to other sample shapes or sample magnetization profiles.

A generic, schematic illustration of the experimental arrangement and the associated notation is illustrated in Fig. 1. The system is based on the use of pick-up coils wound in series opposition that move vertically from one side of the sample to the other. The center of the sample is constrained to lie on the symmetry axis of the sensing coils, which are composed of one layer of copper wire and are identical in construction but wound in series opposition. A relative motion between the sample and the sensing coils gives rise to a flux change in the latter and thus to a voltage signal via Faraday's law, which may then be detected. The magnetic moment can then be determined by direct integration of the electromotive force (e.m.f.) signal generated. The contributions to this integral arising from the dipole, quadrupole, and octupole components of the flux generated by an arbitrary sample are calculated. These results will allow conclusions about the dimensions of the sensing coils and the integration bounds to be drawn in order to ensure the accuracy of the measurement. An appropriate validation technique is described in order to support the results of the measurement system constructed using this approach. The measurement of magnetic relaxation by flux creep in bulk HTS samples is presented, finally, to demonstrate the sensitivity of the device.

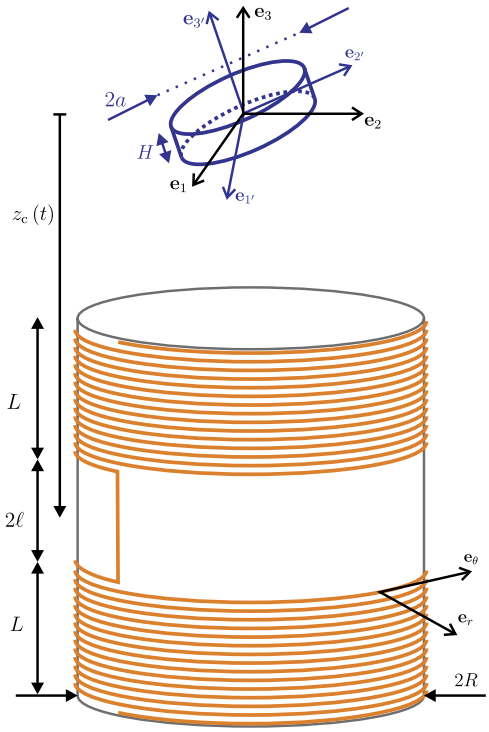

FIG. 1. Schematic illustration of the experimental arrangement: the sample (top, in blue) induces a flux change in the sensing coils (bottom, in orange) when they move along the $\mathbf{e}_3$-axis. In this figure, ($\mathbf{e}_1$, $\mathbf{e}_2$, $\mathbf{e}_3$) (respectively, ($\mathbf{e}_{1'}$, $\mathbf{e}_{2'}$, $\mathbf{e}_{3'}$)) is an orthonormal vector basis whose orientation along $\mathbf{e}_3$ (respectively, $\mathbf{e}_{3'}$) lies along the symmetry axis of the sensing coils (respectively, the sample). They are separated in the figure in order to illustrate the general developments described in Sec. II. In practice, however, the alignment of the sample requires $\mathbf{e}_3 = \mathbf{e}_{3'}$.

II. THEORETICAL BASIS: MULTIPOLE EXPANSION

Integration of the voltage across the sensing coils of a flux extraction magnetometer yields, by Faraday's law, the difference in magnetic flux in the sensing coils between initial and final values. The magnetic flux, therefore, is of prime interest in the measurement of magnetic moment and will be evaluated here using a multipole expansion in order to take into account possible near-field effects in a general way. $\mathbf{B}(\mathbf{r})$ and $\mathbf{A}(\mathbf{r})$ denote the flux density and vector potential, at position $\mathbf{r}$. Using Stokes' theorem, the magnetic flux induced in a single coil of surface $\mathcal{S}$ (normal $\mathbf{n}$) and contour C is given by

$$\int_{\mathcal{S}} \mathbf{B}\cdot\mathbf{n}\,\mathrm{d}\mathcal{S} = \int_{\mathcal{S}} (\nabla\times\mathbf{A})\cdot\mathbf{n}\,\mathrm{d}\mathcal{S} = \oint_C \mathbf{A}\cdot\mathrm{d}\mathbf{l}.$$

For a given position z_c of the sensing coils relative to the sample (see Fig. 1), the total magnetic flux Φ is given by

$$\Phi(z_c) = n\int_{z_c-\ell-L}^{z_c-\ell}\int_0^{2\pi} \mathbf{A}(R\mathbf{e}_r + z\mathbf{e}_3)\cdot R\mathbf{e}_\theta\,\mathrm{d}\theta\,\mathrm{d}z - n\int_{z_c+\ell}^{z_c+\ell+L}\int_0^{2\pi} \mathbf{A}(R\mathbf{e}_r + z\mathbf{e}_3)\cdot R\mathbf{e}_\theta\,\mathrm{d}\theta\,\mathrm{d}z, \quad (1)$$

where n is the number of turns per unit length.

The vector potential depends on the sample, its size, and its shape according to[32,33]

$$\mathbf{A}(\mathbf{r}) = \frac{\mu_0}{4\pi}\int_{\mathbb{V}} \frac{\mathbf{J}(\mathbf{r}')}{|\mathbf{r}-\mathbf{r}'|}\mathrm{d}^3\mathbf{r}', \quad (2)$$

where $\mathbf{J}(\mathbf{r}')$ is the current density in the sample volume $\mathbb{V}$ (using the Coulomb gauge). The effective current density[32] $\mathbf{J}_\mathrm{M} = \nabla' \times \mathbf{M}$ can be used in (2) in the case of a distribution of microscopic magnetization $\mathbf{M}(\mathbf{r}')$ within the sample. The magnetic field around the sample may thus deviate from pure dipole behavior and this relation accounts for these effects. A multipole expansion[31,32] of (2) up to and including the octupole terms is used in order to take such a deviation into account in a general way. Using index notations, this yields

$$\begin{aligned} A_i(\mathbf{r}) &= \frac{\mu_0}{4\pi}\int_{\mathbb{V}} J_i(\mathbf{r}')\left[\zeta_0(\mathbf{r}) + r'_j[\zeta_1(\mathbf{r})]_j \right. \\ &\quad \left. + \frac{r'_j r'_k}{2!}[\zeta_2(\mathbf{r})]_{jk} + \frac{r'_j r'_k r'_l}{3!}[\zeta_3(\mathbf{r})]_{jkl} + \cdots\right] \mathrm{d}^3\mathbf{r}' \\ &= A_i^\mathrm{m}(\mathbf{r}) + A_i^\mathrm{d}(\mathbf{r}) + A_i^\mathrm{q}(\mathbf{r}) + A_i^\mathrm{o}(\mathbf{r}) + \cdots. \end{aligned} \tag{3}$$

In the present work, the superscripts m, d, q, and o represent the monopole, dipole, quadrupole, and octupole contributions, respectively. Note that the monopole contribution $\mathbf{A}^\mathrm{m}$ can be shown easily to be strictly zero, since $\nabla' \cdot \mathbf{J} = 0$. The $\zeta_n(\mathbf{r})$ functions are defined by

$$\zeta_0(\mathbf{r}) = \frac{1}{|\mathbf{r}|}, \tag{4a}$$

$$[\zeta_1(\mathbf{r})]_j = -\frac{\partial}{\partial r_j}\zeta_0 = \frac{r_j}{|\mathbf{r}|^3}, \tag{4b}$$

$$[\zeta_2(\mathbf{r})]_{jk} = -\frac{\partial}{\partial r_k}[\zeta_1]_j = \frac{3r_j r_k}{|\mathbf{r}|^5} - \frac{\delta_{jk}}{|\mathbf{r}|^3}, \tag{4c}$$

$$\begin{aligned}[\zeta_3(\mathbf{r})]_{jkl} &= -\frac{\partial}{\partial r_l}[\zeta_2]_{jk} \\ &= \frac{15 r_j r_k r_l}{|\mathbf{r}|^7} - \frac{3\left(\delta_{jk}r_l + \delta_{jl}r_k + \delta_{kl}r_j\right)}{|\mathbf{r}|^5}. \end{aligned} \tag{4d}$$

Total flux (1) can then be expressed in the form of its component parts

$$\Phi(z_\mathrm{c}) = \Phi^\mathrm{d}(z_\mathrm{c}) + \Phi^\mathrm{q}(z_\mathrm{c}) + \Phi^\mathrm{o}(z_\mathrm{c}) + \cdots, \tag{5}$$

where the first three terms are calculated explicitly in the Appendix. The dipole, quadrupole, and octupole contributions are then given by

$$\Phi^\mathrm{d}(z_\mathrm{c}) = n\frac{\mu_0}{2}\mathbf{m}\cdot\mathbf{e}_3 F^\mathrm{d}(z_\mathrm{c}), \tag{6a}$$

$$\Phi^\mathrm{q}(z_\mathrm{c}) = n\frac{\mu_0}{4R}\mathbf{Q} : \mathbf{e}_3\mathbf{e}_3 F^\mathrm{q}(z_\mathrm{c}), \tag{6b}$$

$$\Phi^\mathrm{o}(z_\mathrm{c}) = n\frac{3\mu_0}{32R^2}\mathbf{O}\dot{:}\left(\mathbf{e}_3(\mathbf{I} - 5\mathbf{e}_3\mathbf{e}_3)\right) F^\mathrm{o}(z_\mathrm{c}), \tag{6c}$$

where $\dot{:}$ (respectively, :) holds for contraction products between third-order (respectively, second-order) tensors, i.e., $\mathbf{T}\dot{:}\mathbf{V} = T_{ijk}V_{ijk}$ if $\mathbf{T}$ and $\mathbf{V}$ are both third-order tensors. In these expressions, $\mathbf{m}$, $\mathbf{Q}$, and $\mathbf{O}$ hold for the dipole, quadrupole, and octupole magnetic moments of the sample, respectively, which are defined as

$$\mathbf{m} = \frac{1}{2}\int_{\mathbb{V}} \mathbf{r}'\times\mathbf{J}\,\mathrm{d}^3\mathbf{r}', \tag{7a}$$

$$\mathbf{Q} = \int_{\mathbb{V}} (\mathbf{r}'\times\mathbf{J})\,\mathbf{r}'\,\mathrm{d}^3\mathbf{r}', \tag{7b}$$

$$\mathbf{O} = \int_{\mathbb{V}} (\mathbf{r}'\times\mathbf{J})\,\mathbf{r}'\mathbf{r}'\,\mathrm{d}^3\mathbf{r}', \tag{7c}$$

and the dimensionless multipole profile functions are given by

$$F^\mathrm{d}(z) = \left[\xi/\left(R^2+\xi^2\right)^{1/2}\right]_{\xi=z-\ell-L;\,z+\ell+L}^{\xi=z-\ell;\,z+\ell}, \tag{8a}$$

$$F^\mathrm{q}(z) = \left[R^3/\left(R^2+\xi^2\right)^{3/2}\right]_{\xi=z-\ell-L;\,z+\ell+L}^{\xi=z-\ell;\,z+\ell}, \tag{8b}$$

$$F^\mathrm{o}(z) = \left[\xi R^4/\left(R^2+\xi^2\right)^{5/2}\right]_{\xi=z-\ell-L;\,z+\ell+L}^{\xi=z-\ell;\,z+\ell}, \tag{8c}$$

where $[f(\xi)]_{\xi=c;\,d}^{\xi=a;\,b} = f(a) + f(b) - f(c) - f(d)$.

The above results give the total magnetic flux across the sensing coils in a general way. Indeed, the size of the sample may be comparable to that of the sensing coils, as illustrated in Sec. III. Moreover, there is no hypothesis about the physical phenomenon responsible for the magnetic properties of the sample, whose origin may be microscopic (as in conventional magnetic materials) or macroscopic (as is the case in type-II superconducting permanent magnets).

III. APPROPRIATENESS OF THE APPROACH: A PARTICULAR CASE

In Sec. II, we calculated explicitly the first three terms of the total magnetic flux across the sensing coils, i.e., the dipole, quadrupole, and octupole contributions. In order to assess the quality of such a truncated multipole expansion, we now consider the theoretical case of a cylindrical HTS sample whose critical current density J_c is assumed to be field-independent. Isotropy and homogeneity are also assumed for this theoretical case. According to Bean's model,[34] the current density within the sample may be described by

$$\mathbf{J}(\mathbf{r}') = \begin{cases} J_\mathrm{c}\mathbf{e}_{\theta'} & \text{if } \mathbf{r}'\cdot\mathbf{e}_{r'} \le a \text{ and } |\mathbf{r}'\cdot\mathbf{e}_{3'}| \le H/2, \\ \mathbf{0} & \text{else,} \end{cases} \tag{9}$$

where a and H are the radius and height of the sample (see Fig. 1), if the sample is fully penetrated. When the symmetry axes of the sample and the sensing coils coincide (i.e., $\mathbf{e}_{3'} = \mathbf{e}_3$), an analytical derivation of the voltage signal over the sensing coils is possible from the knowledge of the mutual inductance between two coaxial circular turns,[35] which yields

$$\text{e.m.f.}(t) = -n\frac{\mathrm{d}z_\mathrm{c}}{\mathrm{d}t}J_\mathrm{c}\left[q(\eta)\right]_{\eta=z_\mathrm{c}+\ell+L;\,z_\mathrm{c}-\ell-L}^{\eta=z_\mathrm{c}+\ell;\,z_\mathrm{c}-\ell}, \tag{10}$$

where

$$q(\eta) = \int_0^a\int_{\eta-H/2}^{\eta+H/2}\sqrt{Rr}\left[\left(\frac{2}{k}-k\right)K(k) - \frac{2E(k)}{k}\right]\mathrm{d}\zeta\,\mathrm{d}r$$

and where $k^2 = 4rR/\left(\zeta^2 + (R+r)^2\right)$. The latter relations are, however, of little practical use in the design of the sensing coils, due to the presence of the cumbersome elliptic integrals K and E. The multipole expansion is therefore a better alternative if it proves appropriate.

Based on current density distribution (9) and the definitions of magnetic moments (7), we have

$$\mathbf{m} = \frac{\pi a^3 H J_\mathrm{c}}{3}\mathbf{e}_{3'}, \tag{11a}$$

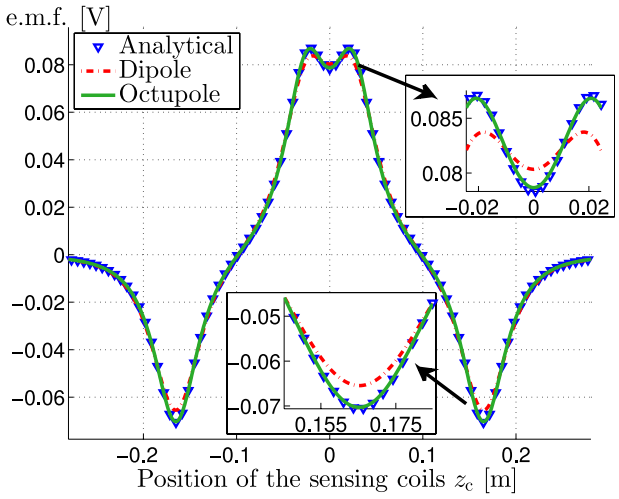

FIG. 2. Theoretical e.m.f. signal for an ideal HTS bulk sample and sensing coils moving at a constant speed $\dot{z}_c = 0.5$ ms^{-1}: comparison between analytical expression (10) and dipole or octupole truncations (12) with the parameters given in Table I. Whereas the dipole truncation (red dashed curve) fails at approximating well the analytical solution (blue triangles), the octupole expansion (green solid curve) constitutes a good fit, as shown by the insets.

$$\mathbf{Q} = \mathbf{0}\,, \tag{11b}$$

$$\mathbf{O} = \frac{\pi a^3 H J_c}{5}\left[a^2 \mathbf{e}_{3'}(\mathbf{I} - \mathbf{e}_{3'}\mathbf{e}_{3'}) + \frac{5H^2}{9}\mathbf{e}_{3'}\mathbf{e}_{3'}\mathbf{e}_{3'} - \frac{5H^2}{36}\delta_{a'b'}\mathbf{e}_{a'}(\mathbf{e}_{b'}\mathbf{e}_{3'} + \mathbf{e}_{3'}\mathbf{e}_{b'})\right]. \tag{11c}$$

Therefore, octupole expansion (5) can be applied readily to approximate the voltage signal according to

$$\text{e.m.f.}\,(t) \simeq -\frac{\mathrm{d}z_c}{\mathrm{d}t}\frac{\mathrm{d}}{\mathrm{d}z_c}\left(\Phi^{\mathrm{d}} + \Phi^{\mathrm{o}}\right) \tag{12}$$

(note that only the first term remains in the case of a dipole truncation). A comparison between analytical approach (10) and the dipole or octupole approximation is shown graphically in Fig. 2 using numerical parameters given in Table I. In this particular case, the radius of the sample ($a = 2.7$ cm) is chosen specifically to be comparable to that of the sensing coils ($R = 4$ cm). This illustrates deliberately a case of near-field effects (small R/a ratio) in order to enlighten the possible defects of the dipole approximation. The triangle symbols in Fig. 2 show the analytical time-dependence of the measured voltage across the sensing coils when they move at a constant speed. The dashed (respectively, plain) line illustrates the same voltage signal determined according to the method described in Sec. II, but truncated after the dipole (respectively, octupole) term (as shown in the insets to the figure). The octupole correction improves significantly the approximation, making the difference with the analytical solution almost negligible. In this example, the octupole correction reduces the dipole maximum relative error of about 7.3% to less than 0.5%.

TABLE I. Parameters (see Fig. 1) associated with the results illustrated in Fig. 2.

m	a	H	R	L	ℓ	$N = nL$
1 A m^2	2.7 cm	2 cm	4 cm	14 cm	2.5 cm	1200

A similar, comparative analysis was conducted for the particular case of a ferromagnetic cylindrical sample. If the magnetization state of this sample is considered homogeneous, i.e., $\mathbf{M} = M\mathbf{e}_{3'}$, then it can be substituted by an effective surface current density[33] $\mathbf{J}_s = M\mathbf{e}_{\theta'}$ in Eqs. (2) and (7). The conclusions obtained for an ideal HTS bulk sample hold perfectly in such a case. Consequently, it is reasonable to use the octupole expansion in order to design the measurement system.

IV. DESIGN OF THE MEASUREMENT DEVICE

The value of the magnetic moment is deduced from a difference in magnetic flux, i.e., by integrating the e.m.f. induced across the sensing coils. Let z_i and z_f denote the initial and final positions of the sensing coils (along $\mathbf{e}_3$) associated with the bounds of integration. Faraday's law then yields $\Phi(z_i) - \Phi(z_f)$ for the integration and the measurement of the magnetic moment (projected on $\mathbf{e}_3$) is deduced from (6a) via

$$\frac{\Phi(z_i) - \Phi(z_f)}{n\mu_0\left(F^{\mathrm{d}}(z_i) - F^{\mathrm{d}}(z_f)\right)/2}. \tag{13}$$

However, this formulation is exact only for a pure dipole sample: in practice, higher order magnetic moments come into play and are responsible for errors in the measurement.

In this section, we use the general results from Sec. II to determine the dimensions (L, ℓ, and R) of the sensing coils as well as the integration bounds z_i and z_f, with the objective being to interpret the difference in magnetic flux predominantly in terms of the dipole moment of the sample and only weakly dependent on higher order components. Using the octupole truncation, the measured flux difference reads

$$\Phi(z_i) - \Phi(z_f) = \left[\Phi^{\mathrm{d}}(z)\right]_{z_f}^{z_i} + \left[\Phi^{\mathrm{q}}(z)\right]_{z_f}^{z_i} + \left[\Phi^{\mathrm{o}}(z)\right]_{z_f}^{z_i}.$$

Profile functions (8) exhibit a remarkable symmetry pattern.[31] Indeed, the function associated with the contribution of kth order moment is $\frac{\mathrm{d}^k}{\mathrm{d}u^k}\left(\sqrt{1+u^2}\right)$, where $u = z/R$. Consequently, F^{d} and F^{o} are odd functions whereas F^{q} is even. The quadrupole contribution to the flux difference, therefore, vanishes completely if we choose $z_i = -z_f = \hat{z}$. In such a case, the flux difference becomes

$$\Phi(z_i) - \Phi(z_f) = 2\Phi^{\mathrm{d}}(\hat{z}) + 2\Phi^{\mathrm{o}}(\hat{z})\,.$$

The relative error ε associated with the value of the magnetic moment deduced from this measurement is thus given at first order by

$$\varepsilon = \frac{\Phi^{\mathrm{o}}(\hat{z})}{\Phi^{\mathrm{d}}(\hat{z})} = \frac{3}{16R^2}\frac{\mathbf{O}\vdots(\mathbf{e}_3(\mathbf{I} - 5\mathbf{e}_3\mathbf{e}_3))}{\mathbf{m}\cdot\mathbf{e}_3}\frac{F^{\mathrm{o}}(\hat{z};\ell,L,R)}{F^{\mathrm{d}}(\hat{z};\ell,L,R)} \tag{14}$$

based on Eqs. (6) and (8). According to the latter relation, it is tempting to set $\hat{z}$ to a root value of F^{o} in order to reject the relative error to a still higher order (note that the hexadecapole contribution is also rejected given that it is associated with an even profile function). However, such a reasoning is of little practical use because it would not tolerate any defect in the sensing coils, however small. As discussed below, $\hat{z}$ has been set to maximize $\Phi^{\mathrm{d}}(\hat{z})$, corresponding to the positions of

the sensing coils associated with zero-crossing voltage signal (in a pure dipole approach) which is consistent with previous studies.[17,18] According to Eq. (8), the $\hat{z}$-value depends on ℓ, L, and R; it cannot be expressed analytically but is easily determined numerically.

The approach using such bounds of integration is now to determine the dimensions ℓ, L, and R in order to ensure that ε does not exceed some limiting value, for example, 10^{-3}. Based on dimensional arguments and on the specific case of the ideal HTS sample discussed previously (Sec. III), the scaling relation

$$\frac{\mathbf{O}\dot{:}(\mathbf{e}_3(\mathbf{I}-5\mathbf{e}_3\mathbf{e}_3))}{\mathbf{m}\cdot\mathbf{e}_3}\sim a^2 \tag{15}$$

may be used and holds true for samples whose aspect ratio a/H is comparable to 1. In this case, the relative error becomes

$$\varepsilon \simeq \frac{3a^2}{16R^2}\frac{F^{\mathrm{o}}(\hat{z};\ell,L,R)}{F^{\mathrm{d}}(\hat{z};\ell,L,R)} \simeq \frac{1}{5}\frac{a^2}{R^2}G\left(\frac{L}{R},\frac{L}{\ell}\right), \tag{16}$$

where the dimensionless ratio $G = F^{\mathrm{o}}/F^{\mathrm{d}}$ depends on the geometrical dimensions ℓ, L, and R, only through L/R and L/ℓ, due to the Buckingham π theorem (recall that $\hat{z}$ also depends on ℓ, L, and R).

The ratio G can be analyzed readily using (8) and the numerical determination of $\hat{z}$. Its dependence on L/R is illustrated in Fig. 3 for some fixed values of L/ℓ chosen over a wide range. This shows that $|G| < 0.1$ as long as $L/R > 3.5$, regardless of the value of L/ℓ. In such a case, we have

$$\varepsilon < \frac{1}{50}\frac{a^2}{R^2}$$

and the relative error may be bounded by 0.1% subject to the conditions

$$\frac{L}{R} > 3.5 \quad \text{and} \quad \frac{R}{a} > 4.5. \tag{17}$$

The spacing 2ℓ between the sensing coils still remains undetermined and may be fixed by other considerations such as the total available length for positioning the sensing coils

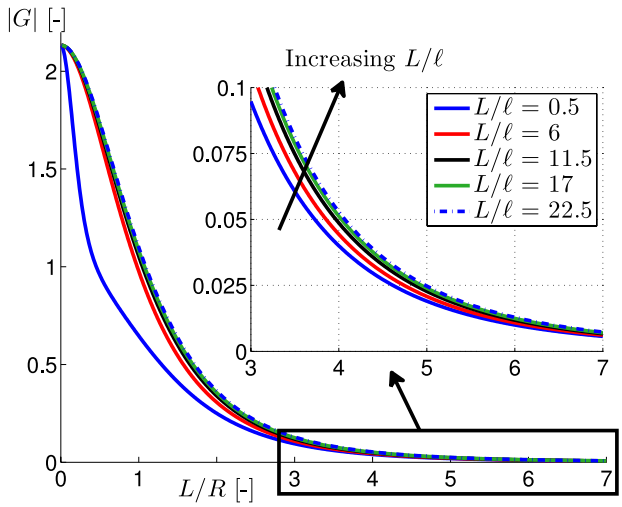

FIG. 3. The absolute value of the dimensionless ratio G as a function of L/R for various values of L/ℓ. The inset shows that $|G| < 0.1$ when $L/R > 3.5$ for a wide range of L/ℓ ratios.

and their displacement. Note also that ℓ is related logically to the coupling between the two sensing coils. In general, the smaller the value ℓ, the stronger the coupling and hence the lower the measured flux difference (and, hence, the sensitivity of the system).

The center of the sample was assumed to be located perfectly on the symmetry axis of the sensing coils throughout this investigation. However, the multipole expansion may again be useful in order to assess the influence of a small displacement $\boldsymbol{\rho}$ of the sample. Such a situation is actually equivalent to a fictitious sample located perfectly, but whose magnetic moments are modified slightly by substituting $\mathbf{r}' + \boldsymbol{\rho}$ for $\mathbf{r}'$ in relations (7). It is well known that this does not change the value of the magnetic moment $\mathbf{m}$. Nevertheless, it results in the addition of $((\mathbf{m}\cdot\boldsymbol{\rho})\mathbf{I} + \mathbf{m}\boldsymbol{\rho})$ to quadrupole moment (7b). Similarly, the ijk-component of the octupole moment then becomes

$$O_{ijk} + Q_{ij}\rho_k + Q_{ik}\rho_j + (\boldsymbol{\rho}\cdot\mathbf{m})\left(\delta_{ij}\rho_k + \delta_{ki}\rho_j\right) + W_{ijk},$$

where $W_{ijk} = \varepsilon_{ipq}\rho_p \int_{\mathbb{V}} J_q r'_j r'_k \,\mathrm{d}^3\mathbf{r}'$. The use of these modifications to the results from Sec. II allows the effects of a small misplacement of the sample to be assessed easily, if required.

V. EXPERIMENTAL SETUP, VALIDATION, AND APPLICATION

The dimensions of the sensing coils may be deduced from the maximum sample radius based on results (17) of Sec. IV. The magnetometer device designed in this work will be used to characterize bulk, superconducting magnets of external diameter less than 1.7 cm. The dimensions

$$L = 14\ \mathrm{cm} \quad \text{and} \quad R = 4\ \mathrm{cm} \tag{18}$$

ensure the efficient measurement of the dipole magnetic moment and the relative contribution of the higher order terms will be less than 0.1%. Sensing coils satisfying those criteria were therefore constructed with one layer of copper wire (100 μm in diameter). The spacing 2ℓ is equal to 5 cm and, importantly, hosts the connections to the data acquisition system.

The creation of two coils of such dimensions with perfect similarity is, in itself, a challenge. In consequence, the number of turns in each sensing coil is not strictly equal but differs from their mean value ($\overline{N}$) of 1223 turns by ±6 units ($\pm\delta N$). Therefore, the symmetry of the integration bounds $z_{\mathrm{i}} = -z_{\mathrm{f}} = \hat{z}$ no longer ensures the quadrupole contribution to the flux difference to be zero. Indeed, taking δN into account and following the reasoning of Sec. II, it can be shown that the quadrupole contribution becomes

$$\frac{\delta N}{L}\frac{\mu_0}{2R}\mathbf{Q}:\mathbf{e}_3\mathbf{e}_3 F^{\mathrm{q}}(\hat{z}). \tag{19}$$

Nevertheless, this does not invalidate the design of the measurement system suggested in Sec. IV since $F^{\mathrm{q}}(\hat{z}) = 0$ because $\hat{z}$ maximizes $F^{\mathrm{d}}(z)$ and $F^{\mathrm{q}}(z) = R\frac{\mathrm{d}}{\mathrm{d}z}F^{\mathrm{d}}(z)$. This would not be the case if $\hat{z}$ was defined as $F^{\mathrm{o}}(\hat{z}) = 0$ and thus justifies the choice for $\hat{z}$, i.e., $F^{\mathrm{q}}(\hat{z}) = 0$.

In the present design, the sample (possibly cooled at cryogenic temperature) is fixed and the sensing coils move

vertically. An electric motor allows the displacement of the sensing coils over a total length of 75 cm at a speed of about 0.5 m/s. Their position along the guiding vertical rail is measured by means of two optical sensors. The first detects a reference position of the coils, while the second measures the time-dependent angular displacement related to the shaft of the motor. A computer running LabView® is used to manage a data acquisition card (NI 6251 DAQ) and to ensure the synchronous acquisition of all signals. The computer then proceeds to data processing in order to compute the time integral of the e.m.f. signal between the well-defined integration bounds $\pm\hat{z}$. These bounds are located accurately due to the digital signals produced by the optical sensors. The voltage offset is measured during the first 200 ms of the measurement process, during which the coils remain at rest. The sample is contained within a polyvinyl chloride (PVC) holder that can be filled with liquid nitrogen. A typical measurement of both the e.m.f. across the sensing coils and their vertical displacement z_c against time is shown in Fig. 4. The sample investigated is a neodymium permanent magnet of 15 mm in diameter and 8 mm in height. The magnetic moment of this sample determined with the system developed here is 1.412 ± 0.002 A m^2.

The measurement procedure relies on the analytical calculations from Sec. II and is expected to be valid within 0.1% relative error providing conditions (17) are fulfilled (the uncertainties due to voltage and position measurements are much smaller than this bound). In theory, therefore, the measurement system requires no calibration procedure under those conditions. Nevertheless, a calibration experiment was performed to assess its accuracy.

Calibration procedures usually make use of standard samples[17,28] made of Ni, MnF_2, Pd, or, more recently, Dy_2O_3. They rely on the well-known magnetic susceptibility of such materials and their associated well-defined magnetization in an externally applied magnetic field. These cannot be used here, however, since no source of external field is used in the system due to its relatively large dimensions.

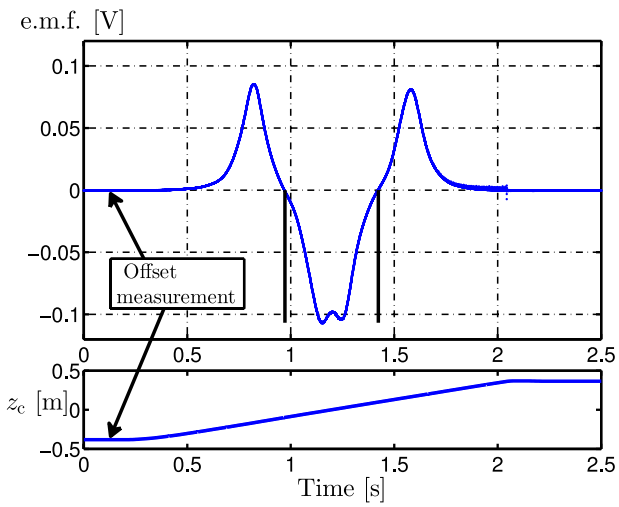

FIG. 4. Top: measured time-dependence of the e.m.f. across the sensing coils. The vertical black lines define the integration bounds. Bottom: concurrent displacement of the sensing coils as a function of time (moving upward).

An alternative way of producing a well-defined magnetic moments is to inject a DC current into a coil to simulate the role of a sample. Therefore, a cylindrical copper coil made of $\mathcal{N} = 57$ turns in one layer was manufactured for this purpose, with the maximum dimensions permitted for the size of the sample holder, i.e., 20 mm in diameter (D) and 18 mm in height. Since D slightly exceeds 17 mm, the maximum relative uncertainty becomes 0.13% rather than 0.1%. By injecting an increasing DC current I into the coil aligned along $\mathbf{e}_3$, reference magnetic moments $\mathbf{m} = \mathcal{N}\pi D^2/4\, I\mathbf{e}_3$ are produced and their uncertainty can be determined from the uncertainties in the current (measured with a Fluke 87 V®) and on the coil diameter. A comparison between these reference magnetic moments and the magnetic moments measured by the system is illustrated in Fig. 5 for DC currents ranging from 0.5 A to 7.5 A, i.e., magnetic moments ranging from 0.009 to 0.131 A m^2. It can be seen that the experimental points lie on the expected straight line within the bounds of uncertainty. This result gives evidence of the correct operation of the system.

In order to assess its sensitivity, the system was finally tested on the measurement of the magnetic relaxation (or "flux creep") into a bulk HTS puck. A cylindrical bulk YBaCuO sample was synthesized by TSMG[36] with a diameter of 16.5 mm and a height of 6.3 mm. The sample was magnetized by field-cooled process using a 1 T Halbach array, and its magnetic moment measured over time for a period of more than 1 h, as illustrated by the blue circles in Fig. 6. This shows the system is sensitive to the observed tiny time-dependent variations of the trapped magnetic moment (less than 1% decrease over more than 1 h).

Some time is required between the end of the magnetizing process and the first measurement given that a field source is not integrated in the current system. Flux creep occurs during this interval so that the first measurement does not represent the maximum trapped magnetic moment. However, it is possible to estimate this value of magnetic moment using a power law time dependence of the following form:

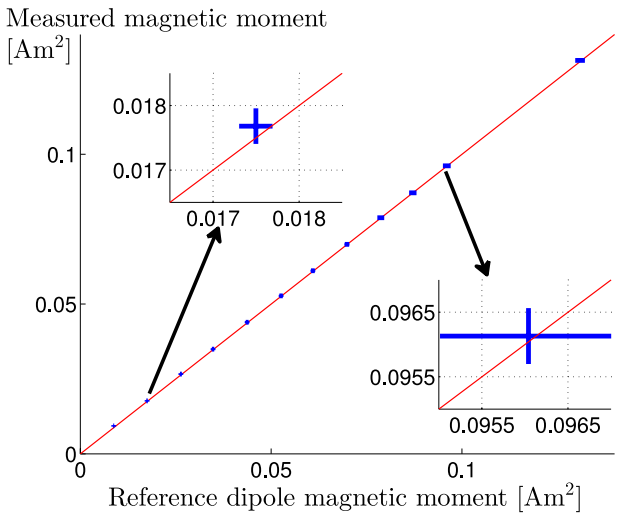

FIG. 5. Magnetic moment measured against the reference magnetic moments produced by an air-cored coil driven by a DC current. The expected behavior (straight line of unity slope) is shown in red; the experimental points and their relative uncertainty bars are shown in blue.

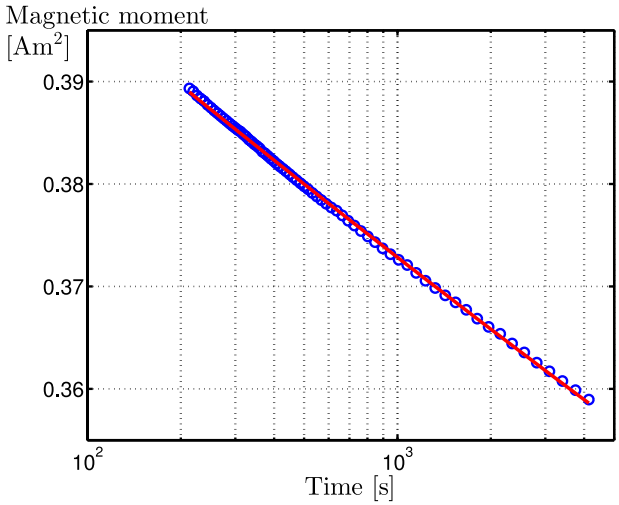

FIG. 6. Measured time-dependence of the magnetic moment of a bulk, large grain YBaCuO HTS sample magnetized permanently by field-cooled process in a 1 T Halbach array. The blue circles are the measured values and the red solid line is a fit to relation (20).

$$m(t) = m_0\left[1 + \frac{t}{t_0}\right]^{\beta} \tag{20}$$

($\beta < 0$) usually observed in flux creep phenomena.[37,38]

The convincing agreement of the measured data with the (red) straight line in the semi-logarithmic plot in Fig. 6 supports this observation. According to (20), m_0 may be a convenient estimation of the maximum trapped magnetic moment, i.e., at the end of the magnetization process. A fit of the experimental data shown in Fig. 6 gives directly $m_0 = 0.431 \pm 0.025$ A m^2. This value is in very good agreement with a previous estimation of 0.432 A m^2, which was deduced from the field-dependent current density distribution obtained by means of numerical methods from the measurement of the e.m.f. induced in a coil wound tightly around the cylindrical bulk superconductor.[13]

Note that several magnetic measurements on large grain YBaCuO materials[13,38] and especially those obtained on small specimens extracted from a large sample [39] showed both axial and radial variations in the critical current density J_c. Therefore, the quadrupole contribution may not be identically zero in this case, unlike that for the simplistic approach addressed in Sec. III. Nevertheless, the good agreement observed above suggests that such a quadrupole effect does not impede the measurement of the magnetic dipole moment, as expected from previous discussion (see Sec. IV and Eq. (19)).

VI. CONCLUSION

An experimental device for the direct and non-destructive measurement of the DC magnetic moment of relatively large samples (up to 17 mm in diameter) has been designed, constructed, and calibrated. The device is based on two pick-up coils wound in series opposition that move linearly over a distance of 75 cm, while the sample, which is magnetized using an external magnetic field, is maintained at constant temperature (which may be cryogenic).

A multipole expansion of the magnetic vector potential has been developed, assessed, and used to establish well-defined conditions concerning the dimensions of the sensing coils for the measurement of the dipole magnetic moment of large samples. The criteria derived are linked inherently to an upper bound on the contribution of moments of higher order to the measured signal. The sensing coils were designed successfully to limit the measurement error to be less than 0.1%. The system has been demonstrated to perform as expected and extends the measurement limits of current maximum magnetic moment of commercial cryogenic magnetic measurement systems to greater than 1 A m^2 (1000 emu). The successful operation of the system is supported by a calibration experiment using reference magnetic moments produced by an air-cored coil (dummy control sample) driven by DC currents. The system has enabled measurements, for the first time, of the remanent volume DC magnetic moment of a whole large bulk YBaCuO sample at liquid nitrogen temperature with a sensitivity that is adequate for probing very small variations of the magnetic moment, such as those occurring during flux-creep.

ACKNOWLEDGMENTS

This work is supported by an *Action de Recherches Concertées* grant from the Ministry of Higher Education through the Research Council of the University of Liège (ARC 11/16-03). The technical help of P. Harmeling and J. Simon is greatly appreciated.

APPENDIX: MULTIPOLE FLUX CONTRIBUTIONS

The main steps of the calculations yielding results (6) are detailed in this Appendix. Let $\phi(z)$ be the elementary flux in a single turn of the sensing coils, which is at the position z relative to the sample. From (3) and (4b), the elementary dipole flux contribution satisfies

$$\phi^{\mathrm{d}}(z) = \frac{\mu_0}{4\pi}\int_{\mathbb{V}} \mathbf{J}\mathbf{r}'\,\mathrm{d}^3\mathbf{r}' : \int_0^{2\pi} R\mathbf{e}_\theta \frac{R\mathbf{e}_r + z\mathbf{e}_z}{(R^2+z^2)^{3/2}}\mathrm{d}\theta. \tag{A1}$$

From symmetry and given that $\mathbf{e}_\theta = \mathbf{e}_3 \times \mathbf{e}_r = \mathbf{e}_a\varepsilon_{a3b}\mathbf{e}_b \cdot \mathbf{e}_r$, where ε_{ijk} is the permutation symbol, the second integral of this expression can be written as

$$\frac{R^2\varepsilon_{a3b}}{(R^2+z^2)^{3/2}}\mathbf{e}_a\mathbf{e}_b \cdot \int_0^{2\pi} \mathbf{e}_r\mathbf{e}_r\,\mathrm{d}\theta = \frac{\pi R^2\varepsilon_{a3b}}{(R^2+z^2)^{3/2}}\mathbf{e}_a\mathbf{e}_b$$

since

$$\int_0^{2\pi} \mathbf{e}_r\mathbf{e}_r\mathrm{d}\theta = \pi\left(\mathbf{e}_1\mathbf{e}_1 + \mathbf{e}_2\mathbf{e}_2\right).$$

Therefore, (A1) can be rewritten as

$$\begin{aligned}\phi^{\mathrm{d}}(z) &= \frac{\mu_0}{4}\frac{R^2}{(R^2+z^2)^{3/2}}\varepsilon_{3ba}\int_{\mathbb{V}} J_a r'_b\,\mathrm{d}^3\mathbf{r}' \\ &= \frac{\mu_0}{2}\frac{R^2}{(R^2+z^2)^{3/2}}\left(\frac{1}{2}\int_{\mathbb{V}} \mathbf{r}'\times\mathbf{J}\,\mathrm{d}^3\mathbf{r}'\right)\cdot\mathbf{e}_3\end{aligned}$$

which yields (6a) when integrated with respect to z as required by (1). A similar reasoning can be applied to the elementary flux of higher order magnetic moments without further obstacle (although the calculations become more involved).

For example, the quadrupole elementary flux involves the following integral calculation:

$$\int_0^{2\pi} R\mathbf{e}_\theta \zeta_2 (R\mathbf{e}_r + z\mathbf{e}_3)\,\mathrm{d}\theta = \int_0^{2\pi} R\mathbf{e}_\theta \frac{3(R\mathbf{e}_r + z\mathbf{e}_3)(R\mathbf{e}_r + z\mathbf{e}_3)}{(R^2+z^2)^{5/2}}\mathrm{d}\theta = \frac{3R^2 z}{(R^2+z^2)^{5/2}}\int_0^{2\pi} (\mathbf{e}_\theta \mathbf{e}_r \mathbf{e}_3 + \mathbf{e}_\theta \mathbf{e}_3 \mathbf{e}_r)\,\mathrm{d}\theta$$
$$= \frac{3R^2 z}{(R^2+z^2)^{5/2}} \mathbf{e}_a \varepsilon_{a3b} \mathbf{e}_b \cdot \int_0^{2\pi} (\mathbf{e}_r \mathbf{e}_r \mathbf{e}_3 + \mathbf{e}_r \mathbf{e}_3 \mathbf{e}_r)\,\mathrm{d}\theta = \frac{3\pi R^2 z}{(R^2+z^2)^{5/2}} \varepsilon_{3ba} \mathbf{e}_a (\mathbf{e}_b \mathbf{e}_3 + \mathbf{e}_3 \mathbf{e}_b)$$

which yields

$$\phi^{\mathrm{q}}(z) = \frac{\mu_0}{8\pi} \frac{3\pi R^2 z}{(R^2+z^2)^{5/2}} \varepsilon_{3ba} \int_{\mathbb{V}} 2 J_a r'_3 r'_b \,\mathrm{d}^3\mathbf{r}' = \frac{3\mu_0}{4} \frac{R^2 z}{(R^2+z^2)^{5/2}} \left(\int_{\mathbb{V}} (\mathbf{r}' \times \mathbf{J})\,\mathbf{r}' \mathrm{d}^3\mathbf{r}' \right) : \mathbf{e}_3 \mathbf{e}_3$$

the integration of which with respect to z as written in (1) leads to (6b).

Similarly, the octupole elementary flux requires the calculation of the rather cumbersome integral

$$\int_0^{2\pi} R\mathbf{e}_\theta \zeta_3 (R\mathbf{e}_r + z\mathbf{e}_3)\,\mathrm{d}\theta = \frac{15R^4}{(R^2+z^2)^{7/2}} \int_0^{2\pi} \mathbf{e}_\theta \mathbf{e}_r \mathbf{e}_r \mathbf{e}_r \mathrm{d}\theta + \frac{15R^2 z^2}{(R^2+z^2)^{7/2}} \int_0^{2\pi} \mathbf{e}_\theta \mathbf{e}_3 \mathbf{e}_3 \mathbf{e}_r + \mathbf{e}_\theta \mathbf{e}_3 \mathbf{e}_r \mathbf{e}_3 + \mathbf{e}_\theta \mathbf{e}_r \mathbf{e}_3 \mathbf{e}_3 \mathrm{d}\theta$$
$$- \frac{3R^2}{(R^2+z^2)^{5/2}} \int_0^{2\pi} \mathbf{e}_\theta \delta_{ab} (\mathbf{e}_a \mathbf{e}_b \mathbf{e}_r + \mathbf{e}_a \mathbf{e}_r \mathbf{e}_b + \mathbf{e}_r \mathbf{e}_a \mathbf{e}_b)\,\mathrm{d}\theta$$
$$= \frac{3\pi R^2 (R^2 - 4z^2)}{4(R^2+z^2)^{7/2}} \varepsilon_{3dc} (\delta_{ab} - 5\delta_{a3}\delta_{b3}) (\mathbf{e}_c \mathbf{e}_a \mathbf{e}_b \mathbf{e}_d + \mathbf{e}_c \mathbf{e}_a \mathbf{e}_d \mathbf{e}_b + \mathbf{e}_c \mathbf{e}_d \mathbf{e}_a \mathbf{e}_b)$$

since $\int_0^{2\pi} \mathbf{e}_r \mathbf{e}_r \mathbf{e}_r \mathbf{e}_r \mathrm{d}\theta = \frac{\pi}{4} (\delta_{ab} - \delta_{a3}\delta_{b3})(\delta_{cd} - \delta_{c3}\delta_{d3})(\mathbf{e}_c \mathbf{e}_d \mathbf{e}_a \mathbf{e}_b + \mathbf{e}_c \mathbf{e}_a \mathbf{e}_d \mathbf{e}_b + \mathbf{e}_c \mathbf{e}_a \mathbf{e}_b \mathbf{e}_d)$. Consequently, the octupole elementary flux is given by

$$\phi^{\mathrm{o}}(z) = \frac{\mu_0}{24\pi} \frac{3\pi R^2 (R^2 - 4z^2)}{4(R^2+z^2)^{7/2}} \varepsilon_{3dc} (\delta_{ab} - 5\delta_{a3}\delta_{b3}) \int_{\mathbb{V}} 3 J_c r'_a r'_b r'_d \,\mathrm{d}^3\mathbf{r}'$$
$$= \frac{3\mu_0}{32} \frac{R^2 (R^2 - 4z^2)}{(R^2+z^2)^{7/2}} \left(\int_{\mathbb{V}} (\mathbf{r}' \times \mathbf{J})\,\mathbf{r}' \mathbf{r}' \mathrm{d}^3\mathbf{r}' \right) \vdots (\mathbf{e}_3 (\mathbf{I} - 5\mathbf{e}_3 \mathbf{e}_3)),$$

where $\mathbf{I}$ is the identity second-order tensor. The integration of this result with respect to z between the bounds of (1) yields (6c).

[1]J. H. Durrell, A. R. Dennis, J. Jaroszynski, M. D. Ainslie, K. G. B. Palmer, Y.-H. Shi, A. M. Campbell, J. Hull, M. Strasik, E. E. Hellstrom, and D. A. Cardwell, Supercond. Sci. Technol. **27**, 082001 (2014).
[2]M. Tomita and M. Murakami, Nature **421**, 517 (2003).
[3]D. Zhou, M. Izumi, M. Miki, B. Felder, T. Ida, and M. Kitano, Supercond. Sci. Technol. **25**, 103001 (2012).
[4]F. Werfel, U. Floegel-Delor, R. Rothfeld, T. Riedel, B. Goebel, D. Wippich, and P. Schirrmeister, Supercond. Sci. Technol. **25**, 014007 (2012).
[5]G. Krabbes, G. Fuchs, W.-R. Canders, H. May, and R. Palka, *High Temperature Superconductor Bulk Materials: Fundamentals, Processing, Properties Control, Application Aspects* (John Wiley & Sons, 2006).
[6]S. Haindl, F. Hengstberger, H. W. Weber, S. Meslin, J. Noudem, and X. Chaud, Supercond. Sci. Technol. **19**, 108 (2006).
[7]I. Chen, J. Liu, R. Weinstein, and K. Lau, J. Appl. Phys. **72**, 1013 (1992).
[8]T. Higuchi, N. Sakai, M. Murakami, and M. Hashimoto, IEEE Trans. Appl. Supercond. **5**, 1818 (1995).
[9]S. Haindl, Supercond. Sci. Technol. **18**, 1483 (2005).
[10]P. Laurent, J. F. Fagnard, B. Vanderheyden, N. H. Babu, D. A. Cardwell, M. Ausloos, and P. Vanderbemden, Meas. Sci. Technol. **19**, 085705 (2008).
[11]M. Raven and M. Salim, Meas. Sci. Technol. **12**, 744 (2001).
[12]P. Vanderbemden, Cryogenics **38**, 839 (1998).
[13]M. Philippe, J.-F. Fagnard, S. Kirsch, Z. Xu, A. Dennis, Y.-H. Shi, D. Cardwell, B. Vanderheyden, and P. Vanderbemden, Phys. C **502**, 20 (2014).
[14]A. Campbell, in *Magnetic Susceptibility of Superconductors and Other Spin Systems*, edited by R. Hein, T. Francavilla, and D. Liebenberg (Springer, US, 1991), pp. 129–155.
[15]S. Foner, Rev. Sci. Instrum. **30**, 548 (1959).
[16]G. J. Bowden, J. Phys. E: Sci. Instrum. **5**, 1115 (1972).
[17]J. K. Krause, IEEE Trans. Magn. **28**, 3066 (1992).
[18]J. Krause, V. Wang, and B. Dodrill, "Magnetic property characterization system employing a single sensing coil arrangement to measure both ac susceptibility and dc magnetization," U.S. patent 5,506,500 (9 April 1996), http://www.google.com/patents/US5506500.
[19]D. Dufeu, E. Eyraud, and P. Lethuillier, Rev. Sci. Instrum. **71**, 458 (2000).
[20]Lake Shore Cryotronics, Inc., 2014, http://www.lakeshore.com/.
[21]Quantum Design, Inc., 2003, http://www.qdusa.com/.
[22]C. L. Foiles and T. W. McDaniel, Rev. Sci. Instrum. **45**, 756 (1974).
[23]E. E. Bragg and M. S. Seehra, J. Phys. E: Sci. Instrum. **9**, 216 (1976).
[24]C. N. Guy, J. Phys. E: Sci. Instrum. **9**, 790 (1976).
[25]A. Zieba and S. Foner, Rev. Sci. Instrum. **53**, 1344 (1982).
[26]J. P. C. Bernards, Rev. Sci. Instrum. **64**, 1918 (1993).
[27]A. Khoder and M. Couach, Cryogenics **31**, 763 (1991).
[28]D.-X. Chen, V. Skumryev, and B. Bozzo, Rev. Sci. Instrum. **82**, 045112 (2011).
[29]B. H. Blott and G. J. Daniell, Meas. Sci. Technol. **4**, 462 (1993).
[30]P. Stamenov and J. M. D. Coey, Rev. Sci. Instrum. **77**, 015106 (2006).
[31]U. Ausserlechner, P. Kasperkovitz, and W. Steiner, Meas. Sci. Technol. **9**, 989 (1998).
[32]J. D. Jackson, *Classical Electrodynamics* (Wiley, New York, 1962), Vol. 3.
[33]D. J. Griffiths and R. College, *Introduction to Electrodynamics* (Prentice hall, Upper Saddle River, NJ, 1999), Vol. 3.
[34]C. P. Bean, Rev. Mod. Phys. **36**, 31 (1964).
[35]E. Durand, *Magnetostatique* (Masson et Cie, Bd St-Germain, Paris (VIe), 1968), Vol. 120 (in French).
[36]N. H. Babu, K. Iida, Y. Shi, and D. Cardwell, Phys. C **445-448**, 286 (2006).
[37]P. Vanderbemden, Z. Hong, T. A. Coombs, S. Denis, M. Ausloos, J. Schwartz, I. B. Rutel, N. H. Babu, D. A. Cardwell, and A. M. Campbell, Phys. Rev. B **75**, 174515 (2007).
[38]D. Cardwell, M. Murakami, M. Zeisberger, W. Gawalek, R. Gonzalez-Arrabal, M. Eisterer, H. Weber, G. Fuchs, G. Krabbes, A. Leenders, H. Freyhardt, X. Chaud, R. Tournier, and N. H. Babu, Phys. C **412–414**(1), 623 (2004).
[39]C. Dewhurst, W. Lo, Y. Shi, and D. Cardwell, Mater. Sci. Eng., B **53**, 169 (1998).